The Astrophysical Journal Letters, 956:L35 (7pp), 2023 October 20 https://doi.org/10.3847/2041-8213/acfe71

One, Two, Three ... An Explosive Outflow in IRAS 12326-6245 Revealed by ALMA

Luis A. Zapata[1], Manuel Fernández-López[2], Silvia Leurini[3], Estrella Guzmán Ccolque[2], I. M. Skretas[4], Luis F. Rodríguez[1], Aina Palau[1], Karl M. Menten[4], and Friedrich Wyrowski[4]
[1] Instituto de Radioastronomía y Astrofísica, Universidad Nacional Autónoma de México, 58090, Morelia, Michoacán, México
[2] Instituto Argentino de Radioastronomía (CCT-La Plata, CONICET; CICPBA), C.C. No. 5, 1894, Villa Elisa, Buenos Aires, Argentina
[3] INAF—Osservatorio Astronomico di Cagliari, Via della Scienza 5, I-09047 Selargius (CA), Italy
[4] Max-Planck-Institut für Radioastronomie, Auf dem Hügel 69, D-53121 Bonn, Germany
Received 2023 August 9; revised 2023 September 17; accepted 2023 September 19; published 2023 October 16

Abstract

In the last years there has been a substantial increase in the number of the reported massive and luminous star-forming regions with related explosive outflows thanks to the superb sensitivity and angular resolution provided by the new radio, infrared, and optical facilities. Here, we report one more explosive outflow related with the massive and bright star-forming region IRAS 12326−6245 using Band 6 sensitive and high-angular-resolution (∼0.″2) Atacama Large Millimeter/Submillimeter Array observations. We find over 10 molecular and collimated well-defined streamers, with Hubble–Lemaitre–like expansion motions, and pointing right to the center of a dusty and molecular shell (reported for the first time here) localized in the northern part of the UC H II region known as G301.1A. The estimated kinematic age and energy for the explosion are ∼700 yr and 10^{48} erg, respectively. Taking into account the recently reported explosive outflows together with IRAS 12326−6245, we estimate an event rate of once every 90 yr in our Galaxy, similar to the formation rate of massive stars.

Unified Astronomy Thesaurus concepts: Star formation (1569)

Supporting material: animation

1. Introduction

Explosive outflows are a relatively new class of molecular outflows related to star-forming regions. These outflows are probably associated with the disruption of a nonhierarchical massive and young stellar system (perhaps triggered by the merger of young massive stars), or with a protostellar collision (e.g., Zapata et al. 2009; Bally et al. 2011; Zapata et al. 2013; Bally 2016; Bally et al. 2017; Raga et al. 2021). The explosive flows are impulsive, and possibly created by a single energetic and brief event (Bally & Zinnecker 2005). These flows consist of dozens of collimated CO streamers, [Fe II] "fingertips," and H_2 wakes pointing back approximately to a central position (see for instance the cases of Orion BN/KL, G5.89−0.39, and IRAS16076−5134; Allen & Burton 1993; Zapata et al. 2009; Bally 2016; Zapata et al. 2020; Guzmán Ccolque et al. 2022), reminiscent of an explosive dispersal event (e.g., Loiseau et al. 2018). The CO streamers, tracing these outflows, are radially distributed, and appear nearly isotropic on the sky, presenting well-defined Hubble–Lemaitre–like velocity gradient along their length. This isotropic distribution makes the red- and blueshifted streamers to appear intertwined, with the CO emission reaching velocity in the line wings of up to 100 km s^{-1}. The energy of these events amounts for over $\sim 10^{48}$ erg, placing them among the most energetic outflows in the galaxy. In the case of Orion BN/KL (the nearest of all these sources) the dynamical ages of most CO streamers are close to 500 yr, exactly the same age of the disruption of a nonhierarchical massive and young stellar system (Gómez et al. 2005; Zapata et al. 2009), which is the event that probably originated the outflow. The disruption of the stellar cluster is clearly traced by the proper motions of at least four stellar objects that recede from the same central position as the molecular gas (Rodríguez et al. 2020). Orion BN/KL is the only case with data from the originating protostellar system, searches for which have so far been elusive in the rest of the cases for now (DR21, G5.89−0.39, S106−IR, IRAS16076−5134: Zapata et al. 2013; Bally et al. 2017; Zapata et al. 2020; Guzmán Ccolque et al. 2022), where the evidence comes form the kinematics of molecular gas.

With the discovery of new explosive outflows associated with massive star-forming regions the estimated rate of events (1 every 100 yr, approximately; see Section 4) is comparable to the rate of supernovae, which indicates that dynamic interactions in highly clustered systems of protostars and even stellar collisions may be a common scenario during the first stages of massive star formation. However, because of the scarcity of these events and the observational challenges that they pose, little is known about the true nature of the engine of these outflows.

The luminous source IRAS12326−6245 (AGAL301.136−00.226 or G301.1364-00.2249) lies at the southern rim of the infrared bubble nebula S169: a semispherical structure of ∼1.2 pc in radius, harboring at least 10 early-type main-sequence stars (Duronea et al. 2021). The usually adopted distance to S169 and IRAS12326−6245 of 4.4 kpc (Osterloh et al. 1997) has recently been revised (Duronea et al. 2021). They showed the association between S169 and the IRAS12326−6245 molecular condensation (named MC3 in their work), proposed a model for the kinematics of the S169 bubble, and estimated a new distance to both structures of $2.03^{+0.77}_{-0.61}$ kpc. In this work, we adopt the 2.03 kpc distance derived by Duronea et al. (2021). We, accordingly, recalculate sizes, luminosities, and other magnitudes extracted from the literature and affected by the change in the distance throughout the text.

The S169 bubble has a dynamical age of 10^5 yr and it is expanding at ∼12 km s^{-1} (Duronea et al. 2021). Its southern

rim is marked by more than 30 protostellar objects detected by Midcourse Space Experiment or Spitzer, product of a probable triggered star formation process. It is delineated by a ridge of dense gas, and harbors a Herschel submillimeter dense dusty core (Duronea et al. 2021). The molecular ridge shows several condensations of gas, of which MC3 contains 5500 $M_{\odot}$ within an area of 0.94 pc, and is very bright in different molecular tracers of dense gas (CS, HNCO; Bronfman et al. 1996; Zinchenko et al. 2000), dust continuum emission (from 1.2 to 0.010 mm; e.g., Henning et al. 2000; Faúndez et al. 2004), and also in the centimeter regime (e.g., Walsh et al. 1998; Urquhart et al. 2007). Through higher-angular-resolution observations, the MC3 molecular condensation is resolved into two mid-infrared (MIR) continuum sources (Henning et al. 2000), coincident with two UC H II regions (Walsh et al. 1998). The southern of these two sources matches the peak position of the IRAS12326−6245 source, with a luminosity of 8.1×10^4 $L_{\odot}$ (Zinchenko et al. 1995; Osterloh et al. 1997).

In addition, IRAS12326−6245 is associated with various high-mass star formation indicators. It shows maser emission from CH_3OH, H_2O, and OH (e.g., MacLeod et al. 1998); single-dish observations show very broad radio recombination lines associated with the UC H II region (FWHM ∼68 km s^{-1}; Araya et al. 2005), and signs of active outflow activity (Henning et al. 2000; Araya et al. 2005).

In this work, we report interferometric CO observations taken with the Atacama Large Millimeter/Submillimeter Array (ALMA) observatory, which show, for the first time, the true nature of the main outflow at the heart of IRAS12326−6245. The ALMA data are part of a survey toward six sources with extremely-high-velocity wings revealed in the APEX spectra, highly indicative of jets, and luminosities $>10^5$ $L_{\odot}$, corresponding to zero-age main-sequence (ZAMS) stars of 20–40 $M_{\odot}$. These ALMA observations are expected to reveal the structure of the flows, and therefore are ideal to test model predictions, and verify whether jets exist in massive young stellar objects. As we will show, these ALMA data have also the capability to reveal the new kind of extreme molecular flows, known as the explosive outflows (Zapata et al. 2009).

We report the telescope setup and the process of image production in Section 2. In Section 3 we present the main results regarding the outflow activity in the region, and finally, Section 4 is dedicated to showing our main conclusions.

2. Observations

The ALMA observations were retrieved from The Science Archive.[5] The observations were carried out during the Cycle 4 science data program 2016.1.01347.S (PI: Silvia Leurini) in 2017 July 20 (with 41 antennas) and 23 (with 44 antennas). This science data program only included 12 m diameter antennas with projected baselines ranging from 16.7 to 3700 m (12.8 to 2846 kλ). The observations were pointed at the phase center located in the sky position $\alpha_{J2000.0} = 12^h35^m35^s.13$, and $\delta_{J2000.0} = 63°02'30''.8$. The IRAS12326−6245 region was completely covered with a small mosaic of seven positions distributed in a Nyquist-sampled grid. The largest angular scale that can be recovered with the present observations is 5″.6. The total integrated time on source was 66 minutes, distributed in the seven-pointing mosaic.

[5] https://almascience.nrao.edu/aq/

The digital correlator was configured with eight spectral windows (SPWs) centered at different frequencies in order to detected different molecular species at these millimeter wave bands. In this work, we concentrate on the SPW1 centered at 230.551 GHz, with a 244.141 kHz width, and divided into 1920 spectral channels, which resulted in a channel spacing of 317 m s^{-1} across the SPW1. This SPW was centered at this frequency to detect the ^{12}CO(2−1) thermal line at a rest frequency of 230.5379700 GHz. We detect strong molecular CO line emission; see Figure 1. We used the eight SPWs to average line-free channels in order to obtain the continuum image. The continuum image is also presented in Figure 1.

The weather conditions were very stable with an average precipitable water vapor of about 0.7 mm and an average system temperature of 100 K. In order to reduce considerably the atmospheric phase oscillation, during the observation simultaneous observation of the 183 GHz water line with water vapor radiometers was included. Quasars J1107−4449, J1252−6737, and J1206−6138 were used to calibrate the bandpass, the atmosphere and the gain fluctuations, and the flux amplitude. Some of the quasar scans were repeated for different calibrations.

To calibrate, image, and analyze the ALMA data we used the Common Astronomy Software Applications (CASA) package, Version 6.4.1.12. Additionally, we also used some routines in Python to analyze the data (Astropy Collaboration et al. 2013). The data were imaged using the routine `TCLEAN` with the Robust parameter set equal to +0.5, a compromise between sensitivity and angular resolution.

We obtained an image of rms noise for the continuum at 1.3 mm of 0.84 mJy beam^{-1} at an angular resolution of $0''.21 \times 0''.18$ with a position angle (PA) of −68°.2. We used a robust equals to 2.0 in `TCLEAN`. This rms value is higher compared with the ALMA theoretical rms noise for this configuration, integration time, bandwidth, and frequency which is approximately 0.08 mJy beam^{-1}. A possibility to explain this, is the presence of a strong UC H II region localized within the field of view (Henning et al. 2000) with an integrated flux of 1.8 Jy, which did not allow us to reach the theoretical noise level; see, for an example, Zapata et al. (2020). Contrary to the continuum noises, we obtained a rms noise for the line images of 2.1 mJy beam^{-1} km s^{-1} at an angular resolution of $0''.18 \times 0''.15$ with a PA of −63°.0 (which translates into a brightness temperature of 1.277 K). We used a robust equals to 0.5 in `TCLEAN`. We obtained similar values for the ALMA theoretical rms noise for the spectral line images.

Using the continuum as a model, we undertook phase self-calibration; we then applied the acquired solutions to the spectral line channels. An improvement of a factor of about 3 in the rms noise was obtained after applying self-calibration.

3. Results

In Figure 1, we show the results of the 1.3 mm continuum and ^{12}CO(2−1) of the ALMA observations toward the massive star-forming regions IRAS12326−6245 and MC3-MIR2. In the continuum emission, we resolve the strong, spherical, and centrally peaked (sub)millimeter source detected with the Large APEX Bolometer Camera (LABOCA) on the APEX telescope (Dedes et al. 2011) toward IRAS12326−6245, and MC3-MIR2, into three compact sources that we name IRAS12326−N, the shell, and IRAS12326−S.

Fitting a Gaussian to IRAS12326−N, we obtain an integrated flux of 138.1 ± 10 mJy, and a peak flux of

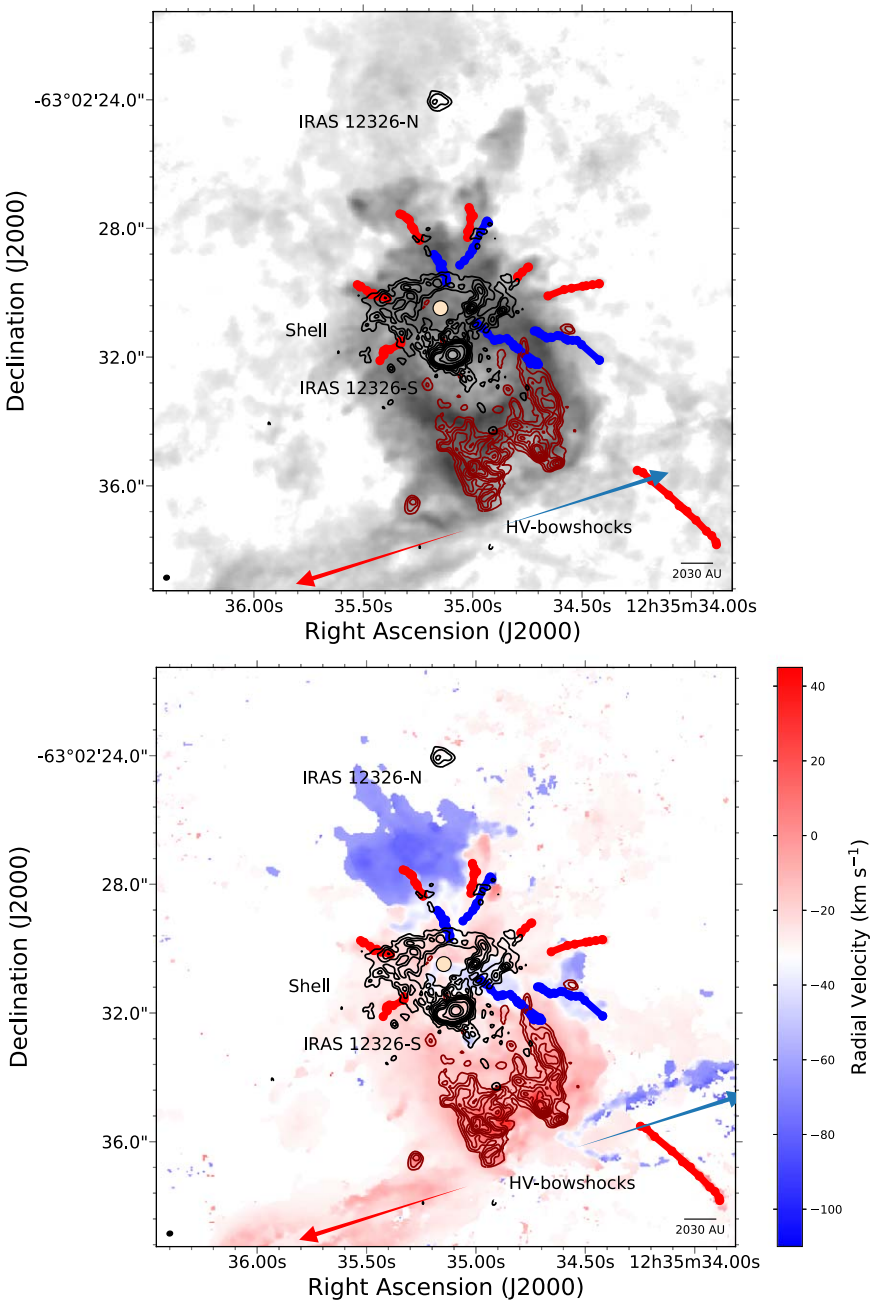

Figure 1. Upper: ALMA ^{12}CO(2−1) moment zero map (gray scale) overlaid with the approaching (in blue colors) and receding (in red colors) explosive streamers discovered in the IRAS12326−6245 molecular outflow, and the 1.3 mm continuum emission (black contours) arising also from this region. The IRAS12326−N source is evident in the north as a compact millimeter continuum source. The black contours are from −6, 6, 10, 15, 20, 25, 30, 40, 50, 100, 250, and 500 × 0.84 mJy beam^{-1}, the rms-noise level of the continuum image. Dark-red contours are tracing the redshifted extremely-high-velocity molecular gas (+70 to +2 km $^{-1}$) with a bow-shock morphology. The contours range from 10% to 100% of the peak emission, in steps of 10%. The peak emission is 0.98 Jy beam^{-1} km s^{-1}. In order to compute the moment zero map for the explosive outflow in IRAS12326−6245, we integrated the radial velocities from −120 to +80 km s^{-1}. On the other hand, we integrated for the blueshifted streamers from −120 to −50 km s^{-1}, and −30 to +80 km s^{-1} for the redshifted ones. The systemic radial velocity is at −39.5 km s^{-1} for the cloud in IRAS12326−6245 (Duronea et al. 2021). The bisque-color circle is tracing the position of the approximate center of the explosive outflow reported in this region. Bottom: same as above but with the ^{12}CO(2−1) moment one map in color scales. The scale-bar on the right shows the radial velocities in km s^{-1}. The animation shows the channel velocity emission from the CO(2−1) line obtained with ALMA from IRAS12326. The radial velocity of every corresponding channel is shown in km s^{-1} in the upper right corner. The time lapse of the animation is 57 s.

(An animation of this figure is available.)

13.0 ± 0.9 mJy beam^{-1}. We also find that the deconvolved size results in a major axis of 685 ± 50 mas, a minor axis of 547 ± 42 mas, and a PA of 27°± 14°. The centroid position in the sky for IRAS12326−N is $\alpha_{J2000.0} = 12^h35^m35^s.155$, and $\delta_{J2000.0} = 63°02'24''.06$. The positional uncertainty for both the decl. and R.A. is about 0″.02. From Figure 1, this source, in particular, seems to be double and possibly multiple. Future observations can resolve better its millimeter emission. This source is coincident with the compact object G301.1364 −00.2249 B, which, based on its 4.8–8.6 GHz spectral index of +0.68, has been classified as a thermal radio jet candidate (Guzmán et al. 2012), and the MIR source HLS2000 MIR 2

(Henning et al. 2000) associated with a dusty object. We obtained a spectral index for IRAS12326−N of +1.9 from the SPWs centered at 216 and 230 GHz, likely associated with dust or optically thick emission from an H II region.

The shell structure is first reported here (Figure 1). This structure encircles the position in the sky $\alpha_{J2000.0} = 12^h35^m35^s142$, and $\delta_{J2000.0} = 63°02'30''.64$, and has an average radius of 3″, though its shape is not exactly round or symmetric. Indeed it is more elongated in the east–west direction (4″.5) than in the north–south direction (about 2.7″). It consists of a series of <0″.5 (1000 au) condensations, and some of its edges seem to comprise various threads or filament-like substructures (see, for instance, two filaments within the western edge). The average width of the dusty shell is about 0″.9 (1800 au). The maximum peak emission from this structure is 30 mJy beam^{-1}, and a flux density of 1.3 Jy, suggesting again that the shell is extended and faint. We estimated a spectral index for one condensation within the shell resulting in +3.1 from the SPWs mentioned before. This indicates that we are seeing optically thin dust emission. Thus a contribution of free–free emission should be minimal at these wavelengths. We estimate the gas and dust mass in the shell by using its flux density and adopting the same assumptions as for the mass estimate of the dust shell in G5.89−0.39 (Fernández-López et al. 2021). That is, we assume optically thin emission, a grain opacity of 0.897 cm^2 g^{-1} (using the measured dust emissivity spectral index $\beta = 1.1$) appropriate for dust with thin ice mantles at densities of 10^6 cm^{-3} (Ossenkopf & Henning 1994), a gas-to-dust ratio of 100, and a temperature ranging from 75 to 150 K. With all of this, we obtain a shell mass ranging between 12.2 and 25.3 $M_\odot$. Under these same assumptions and considering a 20% contamination from free–free emission, we estimate a dust and gas mass for IRAS12326−N between 1.0 and 2.1 $M_\odot$.

Fitting again a Gaussian but now to IRAS12326−S, a strong and compact source just at the southern edge of the shell (see Figure 1) we obtain an integrated flux of 1.87 ± 0.02 Jy, and a peak flux of 1.00 ± 0.03 my beam^{-1}. We also find that the deconvolved size results in a major axis of 300 ± 10 mas, a minor axis of 257 ± 5.0 mas, and a PA of 101° ± 6°. The position in the sky for IRAS12326−S is $\alpha_{J2000.0} = 12^h35^m35^s091$, and $\delta_{J2000.0} = 63°02'31''.92$. The positional uncertainty for both the decl. and R.A. is about 0″.003 (this value is only statistical from the fitting). This source is coincident with the radio compact object G301.1364−00.2249 A, an optically thick UC H II with a spectral index of 2.0 (Walsh et al. 1998; Urquhart et al. 2007; Guzmán et al. 2012). At millimeter wavelengths, we estimated a flat spectral index of −0.15 for this source, which is consistent with an optically thin emission from the UC H II region. The rate of ionizing photons needed to maintain such a UC H II region is ∼2.5 × 10^{48} s^{-1} (Kurtz et al. 1994), which is compatible with a ZAMS star of spectral type O7.5–O8 (Panagia 1973; Martins et al. 2005). The position of this UC H II region is coincident with the dusty shell suggesting a probable relationship with the origin of the explosion as the sources Src I and BN in the Orion-KL region (Zapata et al. 2011). This may imply that the dusty shell, and the UC H II region were probably ejected with a similar acceleration. Some line analysis of the data covered by this ALMA project reveal an east–west velocity gradient ($\Delta V = 15$ km s^{-1}) associated with the dusty shell, which we tentatively associated with an expansion motion. Similar expansion motions are observed in the dusty and ionized shells that surrounds the center of the explosive outflows, see Orion-KL, G5.89 or even DR21 (Zapata et al. 2009, 2013, 2020; Fernández-López et al. 2021). The dynamical age of the shell is estimated to be 700 yr, in very strong agreement with the estimated kinematic age of the explosive outflow.

In Figure 1, we have also included the moment zero, and one maps of the ^{12}CO(2−1) obtained with the present ALMA observations (gray- and color-scale images). In order to compute these maps, we integrated the radial velocities from −120 to +80 km s^{-1}. We remark that with the present sensitive ALMA observations, we find very broad velocity gradient traced by the outflow located here (ΔV ∼200 km s^{-1}). Henning et al. (2000) reported a velocity gradient for this same line of only ΔV ∼80 km s^{-1}, more than a factor of 2 lower. This can be explained by the great sensitivity of the ALMA observations that allows us to detect fainter emission at higher velocities. The CO emission is well resolved as one can see in Figure 1. The CO is tracing two main structures, one to the south, very elongated into an east–west orientation, likely associated with multiple classical bipolar outflows (e.g., Zapata et al. 2015, 2018), and the other one to the north with a morphology resembling an ellipsoidal shell, elongated along a direction with PA ∼ 30°, and centered on or near the position of IRAS 12326-S. The southern rim of this structure coincides with the northern ends of the redshifted bow shocks shown in red contours in Figure 1. We do not find any evidence for an outflow energized by IRAS 12326-N. We also did not find any millimeter or even infrared (IRAC or MIPS in the Spitzer data archive) that could be related with bipolar east–west outflow.

Figure 1 is centered intentionally in the shell-like outflow. In these images, we have additionally overlaid the 10 expansive streamers, and high-velocity redshifted bow-shock structures emanating from a quasi-isotropic outflow reported here for the first time. Each of the streamers traces the position of one sequence of the CO condensations mapped at different radial velocities obtained from the velocity spectral cube. This procedure has been used already in many other studies; see, for example, Zapata et al. (2009, 2013, 2020) and Guzmán Ccolque et al. (2022). In order to get a better view of this procedure, we have made additionally Figure 2. In this figure, we show the moment one map of the CO(2−1) emission from the most southern redshifted expansive filament (see Figure 1) overlaid with the positions of the molecular condensations obtained in the velocity spectral cube together with the radial velocities coded with a color scale similar to that of the radial velocities in the moment one map. From this Figure 2, it is clear to see the great correspondence between the positions of the condensations obtained in the spectral channel cube, and the moment one map. The velocity gradient in Figure 2 is very small (∼10 km s^{-1} over its 3″ length) compared to the full velocity range of the explosion. Thus, given the large projected separation of this streamer from the suspected explosion center, it is likely that most of the motion is close to the plane of the sky. The position on the sky were most of the expansive streamers seem to point is around the center of the dusty shell, at the position $\alpha_{J2000.0} = 12^h35^m35^s147$, and $\delta_{J2000.0} = 63°02'30''.48$ with a positional error of 2″. Unfortunately, we were not able to do a more complete statistical analysis to find the sky center of the explosion due to the low number of explosive streamers. In addition, south of IRAS12326-S we found no clear streamers, probably due to a more dense environment along this direction (which may hamper a clear kinematic and morphological footprint from the collimated streamers). Future sensitive ALMA

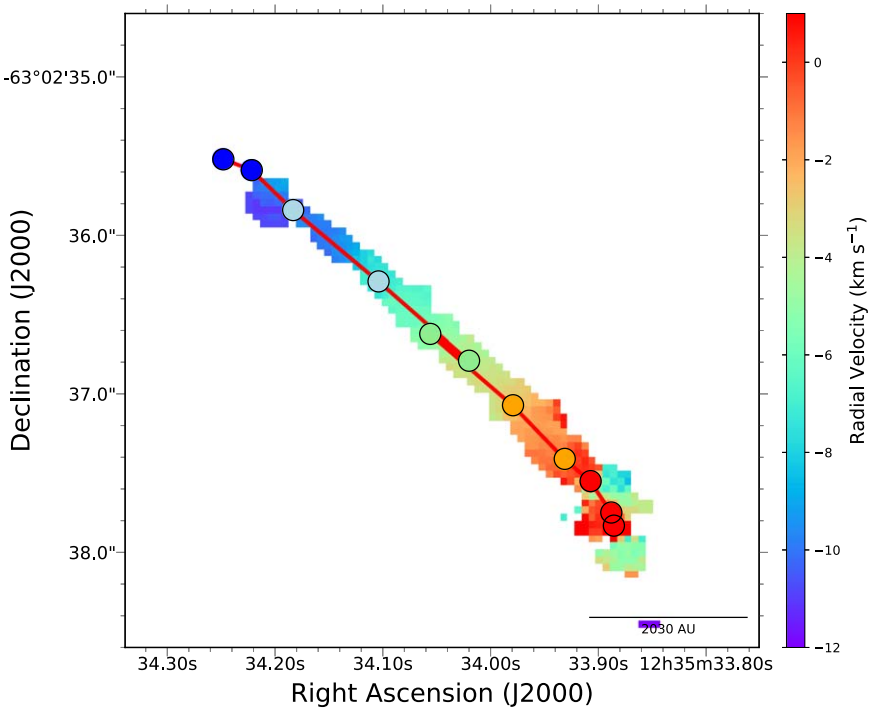

Figure 2. ALMA moment one (color-scale image) overlaid with the positions/radial velocities of the CO(2−1) condensations (color dots) from the most southern redshifted explosive molecular filament (see Figure 1). The filament and the condensations show a clear velocity gradient, with the most redshifted velocities localized far from its origin, i.e., showing Hubble–Lemaitre–like expansion motions. This velocity trend has been observed in other explosive molecular streamers; see, for an example, Zapata et al. (2017).

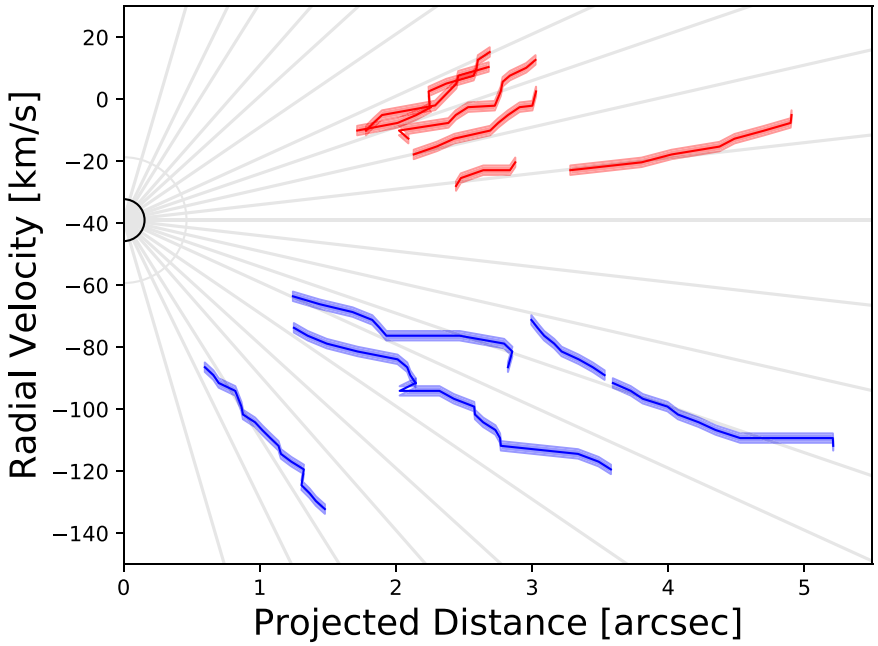

Figure 3. Position−radial velocity diagram of the explosive streamers detected in IRAS12326−6245 with our ALMA observations. The most southern and farther filament shown in Figure 1 is not plotted here for convenience. We have plotted the blueshifted streamers in blue colors, while the redshifted ones in red. All the molecular streamers are mostly pointing to some place around a radial velocity to −39.5 km s^{-1}, the systemic cloud velocity of IRAS12326−6245. In position, the center is located at $\alpha_{J2000.0} = 12^{h}35^{m}35^{s}147$, and $\delta_{J2000.0} = 63°02'30''.48$. In each filament the shaded or blurry blue and red colors represent the error area that is about $0''.1$ for the on-the-sky distance.

observations will likely trace a more complete number of streamers, and the center might be refined.

In Figure 3 is presented the radial velocity versus on-the-sky distance plot of the 10 redshifted and blueshifted expanding streamers reported here. All the 10 streamers follow more or less straight lines and cluster to a range of radial velocities between −20 and −60 km s^{-1}, centered in the LSR systemic velocity of the cloud in IRAS12326−6245, which is −39.5 km s^{-1} (Duronea et al. 2021). Additionally, the expanding streamers also follow Hubble–Lemaitre–like expansion motions, that is, the radial velocities increase with the on-sky-position distances, noted already in many explosive outflows, e.g.,

Zapata et al. (2009, 2013) and Guzmán Ccolque et al. (2022). The physical deviations from straight lines are likely due to internal motions or substructure of the expansive streamers. There is not clear evidence of deceleration in the molecular streamers, likely because of its impulsive nature. From this plot, we can estimate an approximate value for the kinematic time for the outflow, taking an average radial velocity of 40 km s^{-1}, and a distance of 3″ or ∼6000 au, we obtain 700 yr. This kinematic time for the outflow is consistent with the time (800 yr) obtained from the position most southern streamer (8″ away from the origin), and the highest radial velocity observed in the streamers (100 km^{-1}).

In the Appendix section, we have included a PV diagram obtained from the ALMA spectral CO cube, where you can see some of these streamers presented in Figure 3.

Assuming that we are seeing optically thin CO(2−1) emission (more likely the emission is optically thick at these millimeter wavelengths, so this estimation should be considered a lower limit), and that we are in local thermodynamic equilibrium, and following the Equation (2) presented in Cortes-Rangel et al. (2020), we can estimate the mass for the explosive outflow located here. Taking a distance of 2.03 kpc, an excitation temperature of 30 K, a ratio between the molecular hydrogen, and the carbon monoxide of 10^4, and a range of velocities of 120 km s^{-1}, we obtain a mass of 7 $M_\odot$, a momentum of 8×10^2 $M_\odot$ km s^{-1}, and a kinetic energy of 10^{48} erg.

4 Discussion and Conclusions

Our new ALMA observations lead us to propose that in IRAS12326−6245 there is an energetic explosive outflow associated with the shell-like outflow. All the morphological and kinematical features discussed in Zapata et al. (2017) and Guzmán Ccolque et al. (2022) are well distinguished for this outflow. The outflow consists of high-velocity straight narrow filament-like ejections with different orientations; the expansive streamers point back approximately to a common position; the radial velocities from the streamers follow a Hubble–Lemaitre–like expansion; the outflow is embedded in a massive 5500 $M_\odot$ gaseous condensation, and associated with a bright (10^5 $L_\odot$) infrared unresolved IRAS source. This outflow therefore adds one more case to the list of the explosive outflows reported in Orion-KL, DR21, G5.89−0.39, IRAS16076−5134, and S106.

Taking these six explosive outflows reported in the literature (Orion-KL, DR21, G5.89-0.39, IRAS16076−5134, IRAS12326−6245, and S106), we can then estimate the rate of the explosive outflows in our Galaxy. Following Zapata et al. (2020) and Guzmán Ccolque et al. (2022), we can update the rate of explosive outflows in the galaxy. We adopt a time span of 15,330 yr between all six outflows (after taking into account their different distances to Earth), that all of them are immersed within a circle with a radius 2.8 kpc, and that the galaxy is a thin disk with a radius of 15 kpc. With all of this, we estimate an updated rate of events of one every 90 yr. This value is comparable to that reported by Zapata et al. (2020) and Guzmán Ccolque et al. (2022). Our rough estimate will be refined once more explosive outflows will be detected. Moreover, the value reported here is well approximated to the rate of the supernovae, 50 yr (Diehl et al. 2006). Alternatively, we can compare this rate also to the massive star (⩾8 $M_\odot$) formation rate, that can be estimated as follows. The global star formation rate in the Milky Way is ∼2 $M_\odot$ yr^{-1} (Elia et al. 2022). Since the average mass of stars in the initial mass function is ∼0.5 $M_\odot$ (Parravano et al. 2006), we expect that 4 stars form per year. Finally, since the fraction of massive stars is ∼0.5% (Parravano et al. 2006) of the total number of stars, we get a massive star formation rate of 1 star every 50 yr, that not surprisingly is very similar to the supernova formation rate.

In conclusion, we report an explosive outflow localized in the high massive star-forming region know as IRAS12326−6245. We find over 10 molecular and collimated well-defined streamers, with Hubble–Lemaitre–like expansion motions, and pointing right to the center of a dusty shell (reported for the first time here) localized in the northern part of the UC H II region known as MC3-MIR1 or UC H II G301.1A. The estimated kinematic age, mass, and energy for the explosion are ∼700 yr, 7 $M_\odot$, and 10^{48} erg, respectively. Therefore, IRAS12326−6245 adds a new case of explosive outflow as previously observed in Orion-KL, DR21, G5.89-0.39, IRAS16076−5134, and S106.

Acknowledgments

We would like to thank John Bally for his multiple helpful insights into this manuscript. L.A.Z. acknowledges financial support from CONACyT-280775 and UNAM-PAPIIT IN110618, and IN112323 grants, México. A.P. acknowledges financial support from the UNAM-PAPIIT IG100223 grant, and the CONAHCyT project No. 86372 of the "Ciencia de Frontera 2019" program, entitled "Citlalcóatl," México. This paper makes use of the following ALMA data: ADS/JAO. ALMA#2016.1.01347.S. ALMA is a partnership of ESO (representing its member states), NSF (USA) and NINS (Japan), together with NRC (Canada), MOST and ASIAA (Taiwan), and KASI (Republic of Korea), in cooperation with the Republic of Chile. The Joint ALMA Observatory is operated by ESO, AUI/NRAO, and NAOJ. The National Radio Astronomy Observatory is a facility of the National Science Foundation operated under cooperative agreement by Associated Universities, Inc. This research has made use of the SIMBAD database, operated at CDS, Strasbourg, France.

Software: CASA (CASA Team et al. 2022) and astropy (Astropy Collaboration et al. 2013, 2018, 2022).

Appendix

In Figure 4, we show a PV diagram of the ALMA CO(2−1) data. From this Figure, one can see some of the streamers having similar PAs directly from the ALMA data.

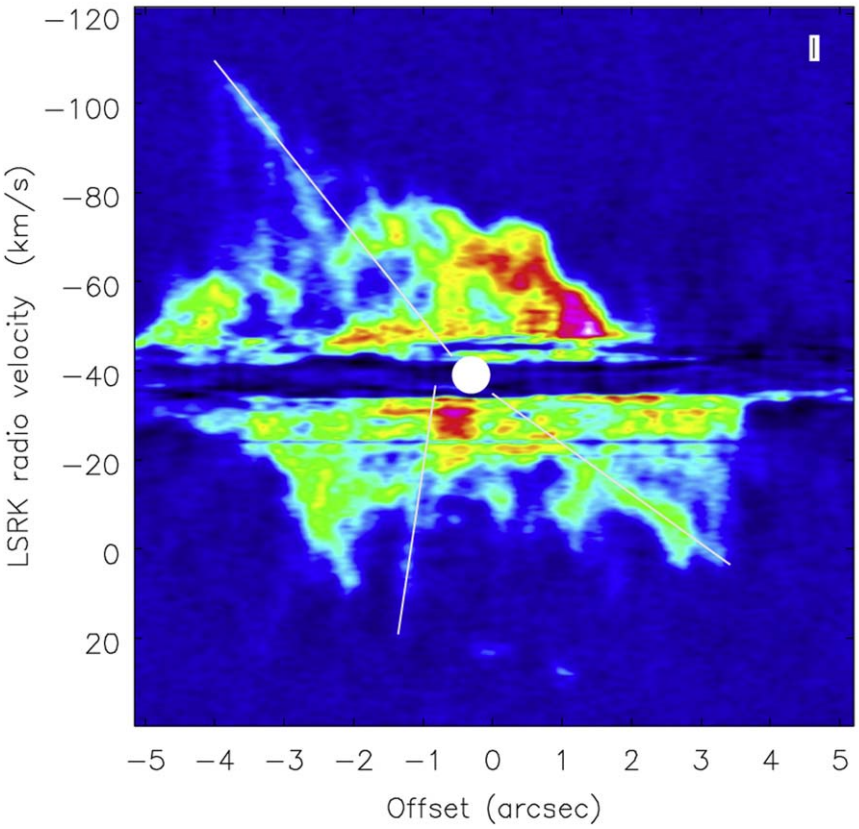

Figure 4. Position−radial velocity diagram of the explosive streamers detected in IRAS12326−6245 with our ALMA observations. The PV diagram is made at the position of the center of the explosion (see text), and a PA of 77°.7. At this PA, we can elucidate three molecular streamers at high velocity. We have marked with white lines the streamers, and with a white circle the center of the explosion.

ORCID iDs

Luis A. Zapata https://orcid.org/0000-0003-2343-7937
Manuel Fernández-López https://orcid.org/0000-0001-5811-0454
Silvia Leurini https://orcid.org/0000-0003-1014-3390
Estrella Guzmán Ccolque https://orcid.org/0000-0003-2630-3774
Luis F. Rodríguez https://orcid.org/0000-0003-2737-5681
Aina, Palau https://orcid.org/0000-0002-9569-9234
Karl M. Menten https://orcid.org/0000-0001-6459-0669
Friedrich, Wyrowski https://orcid.org/0000-0003-4516-3981

References

Allen, D. A., & Burton, M. G. 1993, Natur, 363, 54
Araya, E., Hofner, P., Kurtz, S., Bronfman, L., & DeDeo, S. 2005, ApJS, 157, 279
Astropy Collaboration, Price-Whelan, A. M., Lim, P. L., et al. 2022, ApJ, 935, 167
Astropy Collaboration, Price-Whelan, A. M., Sipőcz, B. M., et al. 2018, AJ, 156, 123
Astropy Collaboration, Robitaille, T. P., Tollerud, E., et al. 2013, A&A, 558, A33
Bally, J. 2016, ARA&A, 54, 491
Bally, J., Cunningham, N. J., Moeckel, N., et al. 2011, ApJ, 727, 113
Bally, J., Ginsburg, A., Arce, H., et al. 2017, ApJ, 837, 60
Bally, J., & Zinnecker, H. 2005, AJ, 129, 2281
Bronfman, L., Nyman, L. A., & May, J. 1996, A&AS, 115, 81
Cortes-Rangel, G., Zapata, L. A., Toalá, J. A., et al. 2020, AJ, 159, 62
CASA Team, Bean, B., Bhatnagar, S., et al. 2022, PASP, 134, 114501
Dedes, C., Leurini, S., Wyrowski, F., et al. 2011, A&A, 526, A59
Diehl, R., Halloin, H., Kretschmer, K., et al. 2006, Natur, 439, 45
Duronea, N. U., Cichowolski, S., Bronfman, L., et al. 2021, A&A, 646, A103
Elia, D., Molinari, S., Schisano, E., et al. 2022, ApJ, 941, 162
Faúndez, S., Bronfman, L., Garay, G., et al. 2004, A&A, 426, 97
Fernández-López, M., Sanhueza, P., Zapata, L. A., et al. 2021, ApJ, 913, 29
Gómez, L., RodrÍguez, L. F., Loinard, L., et al. 2005, ApJ, 635, 1166
Guzmán, A. E., Garay, G., Brooks, K. J., & Voronkov, M. A. 2012, ApJ, 753, 51
Guzmán Ccolque, E., Fernández-López, M., Zapata, L. A., & Baug, T. 2022, ApJ, 937, 51
Henning, T., Lapinov, A., Schreyer, K., Stecklum, B., & Zinchenko, I. 2000, A&A, 364, 613
Kurtz, S., Churchwell, E., & Wood, D. O. S. 1994, ApJS, 91, 659
Loiseau, J., Pontalier, Q., Milne, A. M., Goroshin, S., & Frost, D. L. 2018, ShWav, 28, 473
MacLeod, G. C., Scalise, Eugenio, J., et al. 1998, AJ, 116, 1897
Martins, F., Schaerer, D., & Hillier, D. J. 2005, A&A, 436, 1049
Ossenkopf, V., & Henning, T. 1994, A&A, 291, 943
Osterloh, M., Henning, T., & Launhardt, R. 1997, ApJS, 110, 71
Panagia, N. 1973, AJ, 78, 929
Parravano, A., McKee, C. F., & Hollenbach, D. J. 2006, RMxFS, 52, 1
Raga, A. C., Rivera-Ortiz, P. R., Cantó, J., Rodríguez-González, A., & Castellanos-Ramírez, A. 2021, MNRAS, 508, L74
Rodríguez, L. F., Dzib, S. A., Zapata, L., et al. 2020, ApJ, 892, 82
Urquhart, J. S., Busfield, A. L., Hoare, M. G., et al. 2007, A&A, 461, 11
Walsh, A. J., Burton, M. G., Hyland, A. R., & Robinson, G. 1998, MNRAS, 301, 640
Zapata, L. A., Fernández-López, M., Rodríguez, L. F., et al. 2018, AJ, 156, 239
Zapata, L. A., Ho, P. T. P., Fernández-López, M., et al. 2020, ApJL, 902, L47
Zapata, L. A., Lizano, S., Rodríguez, L. F., et al. 2015, ApJ, 798, 131
Zapata, L. A., Loinard, L., Schmid-Burgk, J., et al. 2011, ApJL, 726, L12
Zapata, L. A., Schmid-Burgk, J., Ho, P. T. P., Rodríguez, L. F., & Menten, K. M. 2009, ApJL, 704, L45
Zapata, L. A., Schmid-Burgk, J., Pérez-Goytia, N., et al. 2013, ApJL, 765, L29
Zapata, L. A., Schmid-Burgk, J., Rodríguez, L. F., Palau, A., & Loinard, L. 2017, ApJ, 836, 133
Zinchenko, I., Henkel, C., & Mao, R. Q. 2000, A&A, 361, 1079
Zinchenko, I., Mattila, K., & Toriseva, M. 1995, A&AS, 111, 95